PERGAMON

International Journal of Heat and Mass Transfer 45 (2002) 4983–4994

International Journal of HEAT and MASS TRANSFER

www.elsevier.com/locate/ijhmt

# Thermocapillary convection with undeformable curved surfaces in open cylinders

Bok-Cheol Sim, Abdelfattah Zebib *

*Department of Mechanical and Aerospace Engineering, Rutgers University, Piscataway, NJ 08854-8058, USA*

Received 7 September 2001; received in revised form 22 May 2002

**Abstract**

Thermocapillary convection driven by a uniform heat flux in an open cylindrical container of unit aspect ratio is investigated by two- and three-dimensional numerical simulations. The undeformable free surface is either flat or curved as determined by the fluid volume ($V \leqslant 1$) and the Young–Laplace equation. Convection is steady and axisymmetric at sufficiently low values of the Reynolds number ($Re$) with either flat or curved interfaces. Only steady convection is possible at any $Re$ in strictly axisymmetric computations. Transition to oscillatory three-dimensional motions occurs as $Re$ increases beyond a critical value dependent on $Pr$ and $V$. Two pulsating and three rotating waves are observed at the free surface with a flat and a concave surface, respectively. The numerical results with either flat or curved free surfaces are in good quantitative agreement with space experiments.


## 1. Introduction

Understanding transition to oscillatory thermocapillary flows is important to material processing in space. Accordingly, there have been a large number of experimental and numerical studies of surface tension driven convection in open rectangular and cylindrical containers. Most of the numerical studies considered thermocapillary convection with flat free surfaces in rectangular cavities, and a few included curved or deformable surfaces in two-dimensional rectangular cavities. Although there are experimental results available for cylindrical containers, numerical studies with curved surfaces in open cylinders appear to have not been performed.

Schwabe et al. [1] studied experimentally thermocapillary flows with $Pr = 17$ in two types of shallow liquid layers heated from the side: one is a rectangular configuration, and the other is an annular slot. In the annular slot heated from the inner rod, they observed azimuthal wavetrains travelling on the free surface, and found that the number of wavetrains increased as $Ma$ increased. Schwabe [2] confirmed the existence of azimuthally travelling wavetrains on the free surface for thin annular gaps.

Kamotani et al. [3,4] investigated experimentally surface tension driven convection with 10 cSt silicone oil induced by two heating modes: one is laser heating with constant heat flux, and the other by a cylindrical heater placed at the center. Their experiments included flat and curved surfaces, which were determined by the liquid volume. However, details of transition were not reported. With 2 cSt silicone oil, Kamotani et al. [5] performed experiments on oscillatory thermocapillary flows in an open cylinder induced by $CO_2$ laser heating. They observed a two-lobed pulsating pattern on the free surface near the onset of oscillations. The pattern remained the same with increasing $Ma$ beyond the critical value. Kamotani et al. [6] considered heating from the inside wall in an open annulus. In their experiments, they found the two-lobed rotating isotherm pattern on the free surface near the onset of oscillations. When $Ma$ was increased, they observed a two-lobed pulsating or a three-lobed pulsating or rotating pattern. In [5,6], $Ma_c$ depended on the container diameter at fixed aspect ratio of 1, so that the onset of oscillations could not be characterized solely by the critical $Ma$. Because previous theories failed to predict this variation of $Ma_c$ with the

* Corresponding author. Tel.: +1-732-445-3268; fax: +1-732-445-3124.

*E-mail address:* zebib@jove.rutgers.edu (A. Zebib).

0017-9310/02/$ - see front matter 
PII: S0017-9310(02)00198-9

**Nomenclature**

| | |
|---|---|
| Ar | aspect ratio, $R/H$ |
| $Ca$ | capillary number, $\gamma T_r/\sigma_0$ |
| $F$ | nondimensional frequency |
| $H$ | height of the cylinder |
| $h$ | heat transfer coefficient |
| $k$ | thermal conductivity |
| $Ma$ | Marangoni number, $PrRe$ |
| $P$ | nondimensional pressure |
| $Pr$ | Prandtl number, $v/\alpha$ |
| $Q$ | heat rate (W) |
| $q$ | nondimensional heat flux |
| $q_0^*$ | average heat flux, $Q/(\pi R^2)$ (W/m$^2$) |
| $R$ | radius of the cylinder |
| $R_h$ | radius of the laser beam |
| $r$ | radial direction |
| $Re$ | Reynolds number, $\gamma(T_rH)/(v\mu)$ |
| $Re_c$ | critical $Re$ |
| $T$ | nondimensional temperature |
| $T_r$ | characteristic $T$, $q_0^*H/k$ |
| $u$ | nondimensional radial velocity |
| $V$ | nondimensional liquid volume |
| $\mathbf{v}$ | nondimensional velocity vector |
| $v$ | nondimensional axial velocity |
| $w$ | nondimensional azimuthal velocity |
| $z$ | axial or vertical direction |

*Greek symbols*

| | |
|---|---|
| $v$ | kinematic viscosity |
| $\mu$ | dynamic viscosity |
| $\alpha$ | thermal diffusivity |
| $\gamma$ | $-\partial\sigma/\partial T$ |
| $\sigma$ | surface tension |
| $\rho$ | density |
| $\theta$ | azimuthal direction |

*Subscript*

| | |
|---|---|
| 0 | reference state |

container diameter, they introduced a critical $S$-parameter which includes effects of free surface deformation. However, Mundrane and Zebib [7] showed that small free surface deformations did not induce transition from steady to oscillatory convection in a model with a low $Pr$ fluid. In addition, Sim and Zebib [8] investigated a model problem using three-dimensional numerical simulations, and found that heat loss from the free surface provided an explanation for $Ma_c$ dependence on the size of the container at fixed aspect ratio as observed in the experiments [6].

Both experimental and three-dimensional numerical studies with $Pr = 6.84$ and various aspect ratios in open annuli were reported by Schwabe et al. [9] and Sim et al. [10]. They found two kinds of azimuthal waves dependent on the aspect ratio: one is travelling clockwise, and the other is pulsating on the free surface. While $Re_c$ was found to decrease with increasing aspect ratio in the case of azimuthally rotating waves, it increased with increasing aspect ratio in the other case. They showed that either heat loss from the free surface or heating from the surroundings to the free surface stabilized the flow, and its inclusion was necessary to achieve better agreement with experiments.

Several numerical studies with curved surfaces have been performed in rectangular cavities. Keller and Bergman [11] and Kamotani and Platt [12] investigated two-dimensional thermocapillary steady convection with undeformable curved surfaces in a cavity. Two-dimensional numerical simulations of steady convection with deforming surfaces in cavities were studied by Liakopoulos and Brown [13] and also Mundrane et al. [14]. Chen et al. [15] and Chen and Hwu [16] considered oscillatory thermocapillary convection with deformable surfaces in cavities.

The effects of curved surfaces on oscillatory convection in open cylindrical containers were reported experimentally by Kamotani et al. [6,17]. They found that $Ma_c$ decreased with increasing liquid volume, i.e., $Ma_c$ with a flat surface was lower than that with a concave surface. Three-dimensional numerical simulations with undeformable curved surfaces appear to have first been performed in a low $Pr$ liquid bridge by Lappa et al. [18].

In the present study, we report on thermocapillary convection with a uniform heat flux in an open cylinder by two- and three-dimensional numerical simulations. The undeformable free surface is either flat or curved. The influence of the free surface shape and $Pr$ on the critical $Re$ and frequency, and the pattern of convection are investigated. Two- and three-dimensional numerical results are then compared with those from available space experiments.

## 2. Mathematical model

The physical system considered is an open cylinder with either flat or curved surface as shown in Fig. 1. It is filled with an incompressible, Newtonian fluid to a height $H$. The aspect ratio ($\mathrm{Ar} = R/H$) of 1 and Prandtl number of 30 and 97 are used to compare numerical predictions with experiments [3,5,17]. A stationary, continuous, axisymmetric laser beam of radius $R_h$ with a uniform heat flux ($Q$) irradiates the surface. The bottom

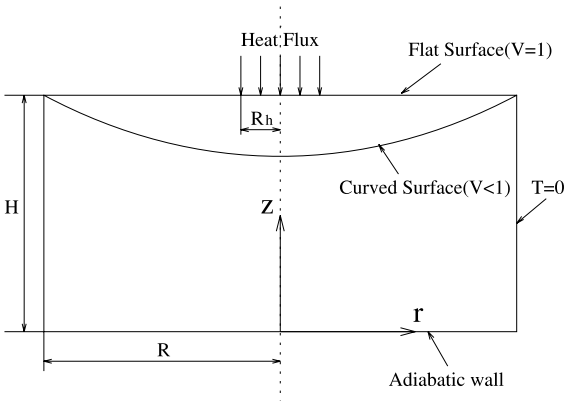


Fig. 1. Physical system.

wall is adiabatic, and the side wall has constant temperature. The surface tension is assumed a linear function of temperature

$$\sigma = \sigma_0 - \gamma(T - T_0). \tag{1}$$

In a microgravity environment, the nondimensional governing equations are as follows:

$$\nabla \cdot \mathbf{v} = 0, \tag{2}$$

$$Re\left(\frac{\partial \mathbf{v}}{\partial t} + \nabla \cdot (\mathbf{v}\mathbf{v})\right) = -\nabla P + \nabla^2 \mathbf{v}, \tag{3}$$

$$Ma\left(\frac{\partial T}{\partial t} + \nabla \cdot (\mathbf{v}T)\right) = \nabla^2 T. \tag{4}$$

Length, temperature, velocity, pressure, and time are normalized with respect to $H$, $T_r$, $\gamma T_r/\mu$, $\gamma T_r/H$, and $\mu H/\gamma T_r$, respectively. The boundary conditions become

$$u = 0, \quad v = 0, \quad w = 0, \quad T = 0, \quad \text{at } r = 1, \tag{5}$$

$$u = 0, \quad v = 0, \quad w = 0, \quad \frac{\partial T}{\partial z} = 0, \quad \text{at } z = 0. \tag{6}$$

The nondimensionalized position of the free surface is described by a function $h(r)$. The heat flux boundary condition, kinematic boundary condition and tangential stress balances at the interface are

$$-\frac{1}{N}\left(h'\frac{\partial T}{\partial r} - \frac{\partial T}{\partial z}\right) = q, \tag{7}$$

$$v = h'u, \tag{8}$$

$$(1 - h'^2)\left(\frac{\partial u}{\partial z} + \frac{\partial v}{\partial r}\right) + 2h'\left(\frac{\partial v}{\partial z} - \frac{\partial u}{\partial r}\right) = -N\left(\frac{\partial T}{\partial r} + h'\frac{\partial T}{\partial z}\right), \tag{9}$$

$$-h'\left(\frac{1}{r}\frac{\partial u}{\partial \theta} - \frac{w}{r} + \frac{\partial w}{\partial r}\right) + \frac{1}{r}\frac{\partial v}{\partial \theta} + \frac{\partial w}{\partial z} = \frac{-N}{r}\frac{\partial T}{\partial \theta}, \tag{10}$$

where $q = 1/H_r^2$ at $r \leqslant H_r$ and $q = 0$ at $r > H_r$, $H_r = R_h/R$, $N = (1 + h'^2)^{1/2}$ and $h' = \mathrm{d}h/\mathrm{d}r$. The tangential stress balances Eqs. (9) and (10) define the driving thermocapillary forces.

The location of the interface, $h(r)$, is determined by the normal stress balance. The deviation of the free surface shape from the static meniscus is characterized by the capillary number, $Ca$. When $Ca \ll 1$, the dynamic surface deformation can be neglected [7], and the normal stress balance equation simplifies to the Young–Laplace equation. The shape of the interface is then fixed with a prescribed liquid volume. The interface and liquid volume equations in a state of rest are as follows:

$$-Ca\Delta P = \frac{1}{N}\left(\frac{h''}{N^2} + \frac{h'}{r}\right), \tag{11}$$

$$V = 2\int_0^1 rh\,\mathrm{d}r, \tag{12}$$

where $\Delta P = P - P_0$ is the nondimensional pressure difference between the interface liquid and gas pressures, and the liquid volume is normalized with respect to $\pi R^2 H$. Eq. (11) with two boundary conditions, $h'(0) = 0$ and $h(1) = 1$, allows an exact solution

$$h(r) = 1 + \frac{1}{C}[(1 - C^2)^{1/2} - (1 - C^2 r^2)^{1/2}], \tag{13}$$

where $C = -Ca\Delta P/2$. If the liquid volume is given, the constant $C$ and the shape of interface, $h(r)$, are determined by Eqs. (12) and (13). In particular, when $V = 1$, $C = 0$ and $h = 1$.

## 3. Numerical aspects

In order to solve the problem with a curved surface, the governing equations are transformed from the physical domain $(r, z, \theta)$ into a rectangular computational domain $(\xi, \eta, \zeta)$.

$$\xi = r, \tag{14}$$

$$\eta = z/h(r), \tag{15}$$

$$\zeta = \theta, \tag{16}$$

The governing equations transformed into the computational domain are

$$\frac{1}{\xi}\frac{\partial \xi u}{\partial \xi} - \eta\frac{h'}{h}\frac{\partial u}{\partial \eta} + \frac{1}{h}\frac{\partial v}{\partial \eta} + \frac{1}{\xi}\frac{\partial w}{\partial \zeta} = 0, \tag{17}$$

$$Re\left[\frac{\partial u}{\partial t} + \frac{1}{\xi}\frac{\partial \xi u^2}{\partial \xi} - \eta\frac{h'}{h}\frac{\partial u^2}{\partial \eta} + \frac{1}{h}\frac{\partial uv}{\partial \eta} + \frac{1}{\xi}\frac{\partial uw}{\partial \zeta} - \frac{w^2}{\xi}\right] = -\frac{\partial p}{\partial \xi} + \eta\frac{h'}{h}\frac{\partial p}{\partial \eta} - \frac{u}{\xi^2} + \nabla^2 u - \frac{2}{\xi^2}\frac{\partial w}{\partial \zeta}, \tag{18}$$

$$Re\left[\frac{\partial v}{\partial t}+\frac{1}{\xi}\frac{\partial \xi uv}{\partial \xi}-\eta\frac{h'}{h}\frac{\partial uv}{\partial \eta}+\frac{1}{h}\frac{\partial v^2}{\partial \eta}+\frac{1}{\xi}\frac{\partial vw}{\partial \zeta}\right] = -\frac{1}{h}\frac{\partial p}{\partial \eta}+\nabla^2 v, \tag{19}$$

$$Re\left[\frac{\partial w}{\partial t}+\frac{1}{\xi}\frac{\partial \xi uw}{\partial \xi}-\eta\frac{h'}{h}\frac{\partial uw}{\partial \eta}+\frac{1}{h}\frac{\partial vw}{\partial \eta}+\frac{1}{\xi}\frac{\partial w^2}{\partial \zeta}+\frac{uw}{\xi}\right] = -\frac{1}{\xi}\frac{\partial p}{\partial \zeta}+\nabla^2 w-\frac{w}{\xi^2}+\frac{2}{\xi^2}\frac{\partial u}{\partial \zeta}, \tag{20}$$

$$PrRe\left[\frac{\partial T}{\partial t}+\frac{1}{\xi}\frac{\partial \xi uT}{\partial \xi}-\eta\frac{h'}{h}\frac{\partial uT}{\partial \eta}+\frac{1}{h}\frac{\partial vT}{\partial \eta}+\frac{1}{\xi}\frac{\partial wT}{\partial \zeta}\right] = \nabla^2 T, \tag{21}$$

$$\nabla^2 = \frac{1}{\xi}\frac{\partial}{\partial \xi}\left(\xi\frac{\partial}{\partial \xi}\right)-\frac{2\eta h'}{h}\frac{\partial^2}{\partial \eta \partial \xi}+\left[2\left(\frac{h'}{h}\right)^2-\frac{h''}{h}-\frac{h'}{h\xi}\right]\times\eta\frac{\partial}{\partial \eta}+\left[\left(\frac{h'\eta}{h}\right)^2+\frac{1}{h^2}\right]\frac{\partial^2}{\partial \eta^2}+\frac{1}{\xi^2}\frac{\partial^2}{\partial \zeta^2}. \tag{22}$$

The transformed boundary conditions become

$$\text{At } \xi=1, \qquad T=0, \quad u=0, \quad v=0, \quad w=0, \tag{23}$$

$$\text{At } \eta=0, \qquad \frac{\partial T}{\partial \eta}=0, \quad u=0, \quad v=0, \quad w=0. \tag{24}$$

At the interface ($\eta=1$),

$$\frac{1+h'^2}{h}\frac{\partial T}{\partial \eta}-h'\frac{\partial T}{\partial \xi}=Nq, \tag{25}$$

$$\left(\frac{1+h'^2}{h}\right)\frac{\partial u}{\partial \eta}-2h'\frac{\partial u}{\partial \xi}+\left(\frac{h'+h'^3}{h}\right)\frac{\partial v}{\partial \eta}+(1-h'^2)\frac{\partial v}{\partial \xi} = -N\frac{\partial T}{\partial \xi}, \tag{26}$$

$$v=h'u, \tag{27}$$

$$\left(\frac{1+h'^2}{h}\right)\frac{\partial w}{\partial \eta}-h'\left(\frac{1}{\xi}\frac{\partial u}{\partial \zeta}+\frac{\partial w}{\partial \xi}\right)+\frac{1}{\xi}\frac{\partial v}{\partial \zeta}=\frac{-N}{\xi}\frac{\partial T}{\partial \zeta}. \tag{28}$$

Periodic boundary conditions are used in the azimuthal direction, while handling the coordinate singularity on the cylinder axis can be found in [19].

First, the shape ($h$) of the interface with described liquid volume is determined by Eq. (13). The transformed governing equations (17)–(21) and boundary conditions equations (23)–(28) are then solved by a finite volume method employing a SIMPLER algorithm. Nonuniform grids are constructed with finer meshes in the regions under the free surface and the laser beam, and near the bottom and side walls where boundary layers develop. In order to examine grid dependence in axisymmetric models, surface velocity and temperature distributions are computed with various grids and liquid volumes, and a mesh of $81(N_r)\times 81(N_z)$ is used. In the three-dimensional model, critical Reynolds numbers, $Re_c$, are computed with various grids. Table 1 shows $Re_c$ and wavenumber found using different grids with various $V$ and $Pr$. The azimuthal direction has uniform grids. $Re$ is varied in increments of 250 ($V=1$) and 1000 ($V=0.81$) in order to estimate $Re_c$. These steps in $Re$ are less than 5% of the reported $Re_c$.

Table 1
Grid refinement studies of three-dimensional convection

| $V$ | $Pr$ | Grid numbers ($N_r\times N_z\times N_\theta$) | $Re_c$ | Wavenumber |
|---|---|---|---|---|
| 1 | 30 | $61\times 61\times 20$ | $5.75\times 10^3$ | 2 |
| | | $61\times 61\times 40$ | $5.75\times 10^3$ | 2 |
| | | $71\times 71\times 28$ | $5.5\times 10^3$ | 2 |
| | 97 | $66\times 66\times 23$ | $8.5\times 10^3$ | 2 |
| | | $71\times 71\times 28$ | $8.5\times 10^3$ | 2 |
| 0.81 | 30 | $61\times 61\times 20$ | $2.3\times 10^4$ | 4 |
| | | $61\times 61\times 40$ | $2.3\times 10^4$ | 3 |
| | | $71\times 71\times 28$ | $2.3\times 10^4$ | 3 |

## 4. Results and discussion

### 4.1. Axisymmetric thermocapillary convection

Surface temperature distribution is compared with the experimental results from Kamotani et al. [3] in Fig. 2. Property values for numerical simulations can be found in [20], and $k=0.134$ W/mK. Axisymmetric numerical results are in good agreement with those from three-dimensional simulations in a steady state as shown in Fig. 2. It is found that a steady state is axisymmetric. While the maximum temperature of the numerical study is about 5% higher than the experimental result, the bulk temperature on the free surface is higher in the experiment. The difference is probably due to the uniform heat flux and adiabatic assumptions on the free surface.

We studied thermocapillary convection with both Prandtl numbers up to $Re=5\times 10^4$. It is found that oscillatory thermocapillary convection with $Pr=30$ and 97 cannot be realized in two-dimensional numerical studies with either flat or curved surfaces. We thus conclude that only azimuthal waves can generate oscillations in thermocapillary convection. This result is very different from those of two-dimensional rectangular cavities reported by Xu and Zebib [21], where oscillatory thermocapillary convection can be investigated in

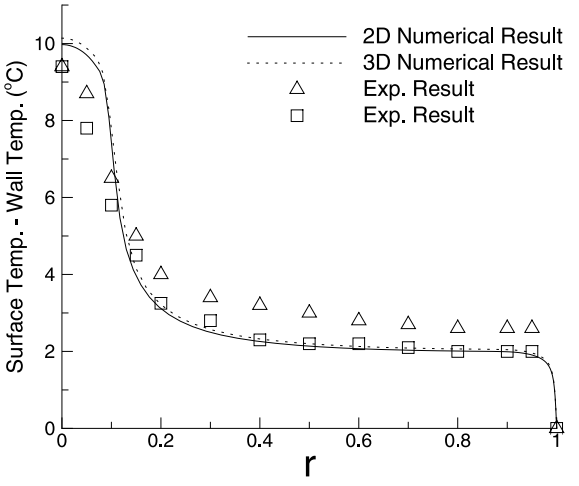


Fig. 2. Surface temperature distribution with $Pr = 97$ and $Re = 830$ ($Q = 0.48$ W). A steady state is axisymmetric.

two-dimensional simulations. While oscillatory buoyant–thermocapillary convection in liquid bridges was reported with axisymmetric numerical simulations, oscillatory thermocapillary convection was not found in the simulations [20].

Fig. 3 shows isotherms and streamlines with a flat surface and various *Re*. The surface velocity and temperature distributions are shown in Fig. 4. The maximum velocity and temperature decrease with increasing *Re*. Because the surface temperature gradient is larger at lower *Re*, the velocity is faster, and the maximum value of streamlines is higher at lower *Re*. The center of recirculations cells moves closer to the cold wall with increasing *Re*. The bulk temperature of the liquid increases with decreasing *Re* indicating more vigorous convection. Fig. 5 shows isotherms and streamlines with a curved surface, $V = 0.81$. The surface velocity and temperature distributions corresponding to Fig. 5 are shown in Fig. 6. When compared with the case of $V = 1$ at the same *Re*, while the surface velocities near the middle of the surface are much higher, the velocities near the side wall are much lower. Maximum surface velocity and temperature are roughly the same as those of the flat surface. The maximum value of the stream functions with $V = 0.81$ is much larger indicating higher velocities. Because the flow patterns with $Pr = 97$ are similar to the case with $Pr = 30$, the plots are omitted.

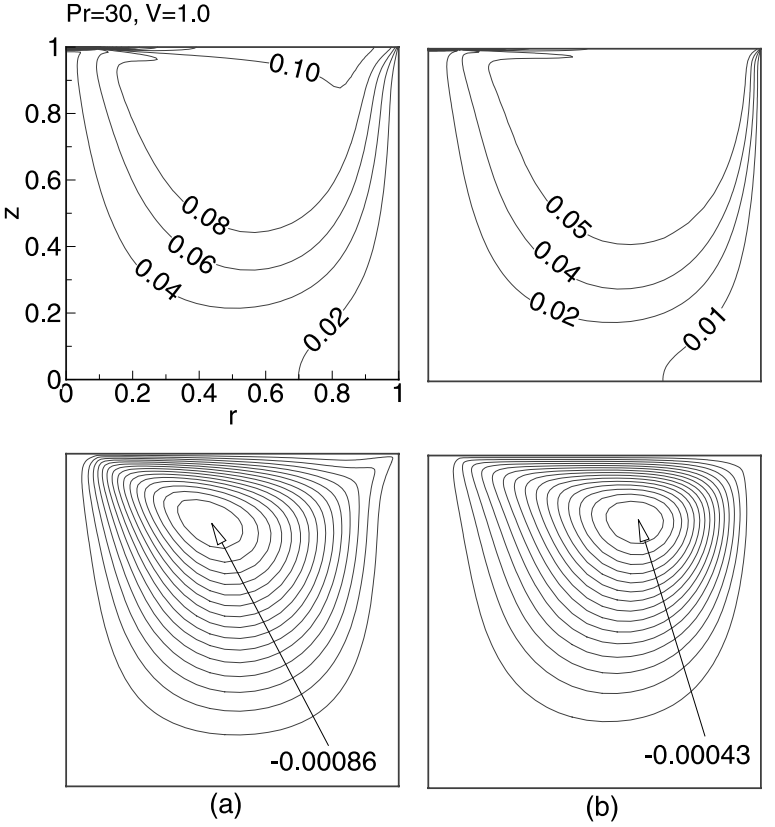


Fig. 3. Isotherms and streamlines with $Pr = 30$, $V = 1$ and (a) $Re = 1 \times 10^3$, (b) $Re = 1 \times 10^4$. The maximum value of streamlines decreases with increasing *Re*.

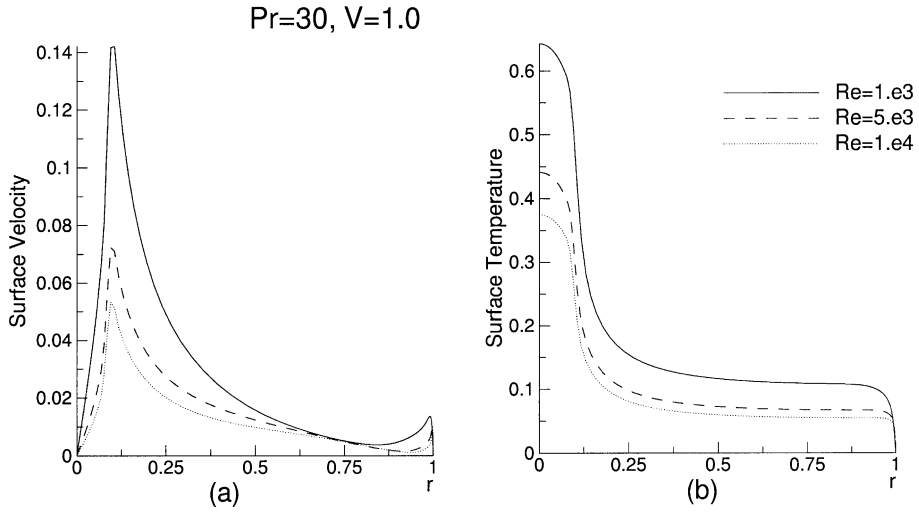


Fig. 4. Surface (a) velocity and (b) temperature corresponding to the flows in Fig. 3. Surface velocity and temperature decreases with increasing *Re*.

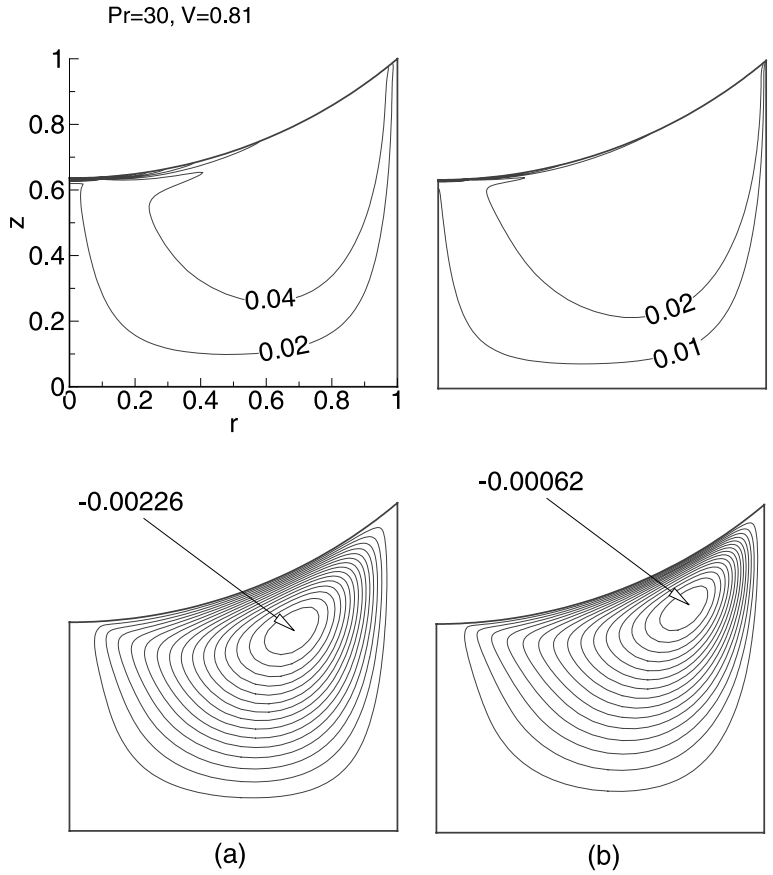


Fig. 5. Isotherms and streamlines with $Pr = 30$, $V = 0.81$ and (a) $Re = 1 \times 10^3$, (b) $Re = 1 \times 10^4$.

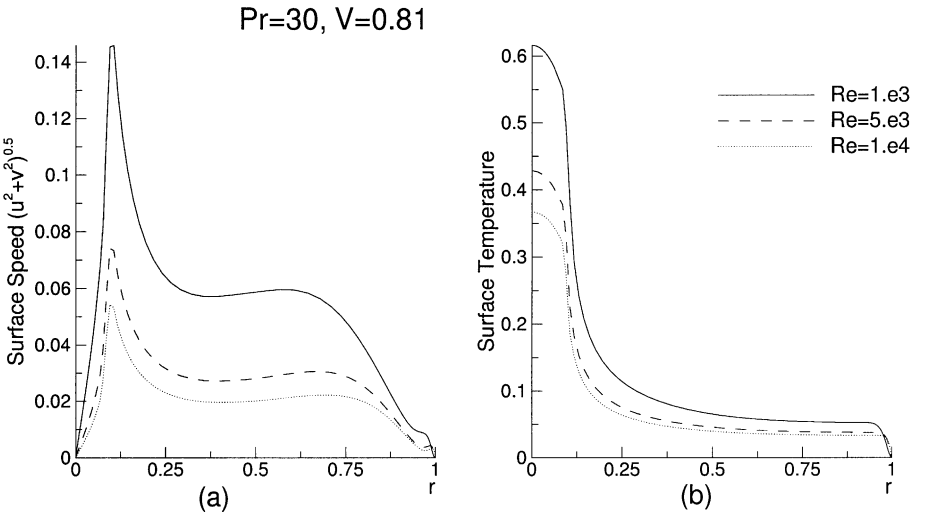


Fig. 6. Surface (a) velocity and (b) temperature corresponding to the flows in Fig. 5. The maxima are about equal to those with $V = 1$ in Fig. 4.

### 4.2. Three-dimensional thermocapillary convection with a flat surface

$Re_c$ for onset of oscillations with $Pr = 30$ is about $5.75 \times 10^3$, which is well within the range ($3.8 \times 10^3$–$1.15 \times 10^4$) found in the experiments [5]. At this critical $Re$, the flow is steady and the isotherms on the free surface are just circular lines, i.e. axisymmetric. Fig. 7 shows the time history of the temperature near the mid-point of the free surface at three supercritical $Re$ values. Fig. 7(a–c) are computed from the same steady state initial conditions. As expected, oscillations begin earlier in time at the higher $Re$. While the amplitudes of temperature oscillations are larger at the higher $Re$, the mean temperature at these points decreases with increasing $Re$. Frequency ($F$), calculated by a Fourier decomposition of the temperature signal at a fixed point, decreases with increasing $Re$.

Fig. 8 shows isotherms corresponding to four instants of the temperature oscillations at the free surface in one cycle with $Re = 6.25 \times 10^3$. It can be seen that the two-lobed wave is pulsating twice for one cycle with two azimuthal waves. Thus the frequency of the temperature will be half of the isotherm pulsating frequency. This is in good agreement with the experimental results [5].

In order to show the main features of the oscillations, the temperature fluctuations, i.e. deviation from the time-averaged mean temperature at each position on the free surface, are shown in Fig. 9. Figs. 8 and 9 are at the same instant. Temperature fluctuations in Fig. 9

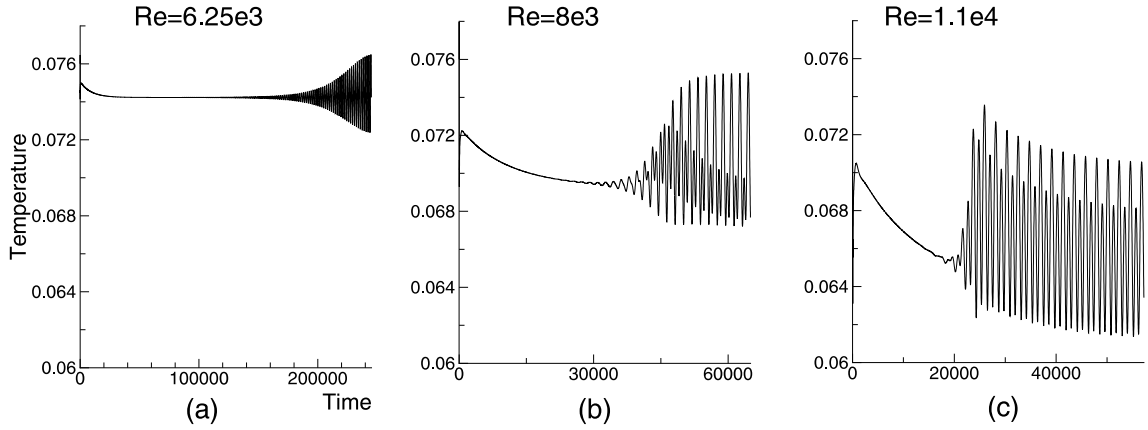


Fig. 7. Time history of the temperature near the mid-point of the free surface with $V = 1$, $Pr = 30$ and three supercritical $Re$. Starting from the same initial conditions, oscillations begin earlier in time at the higher $Re$.

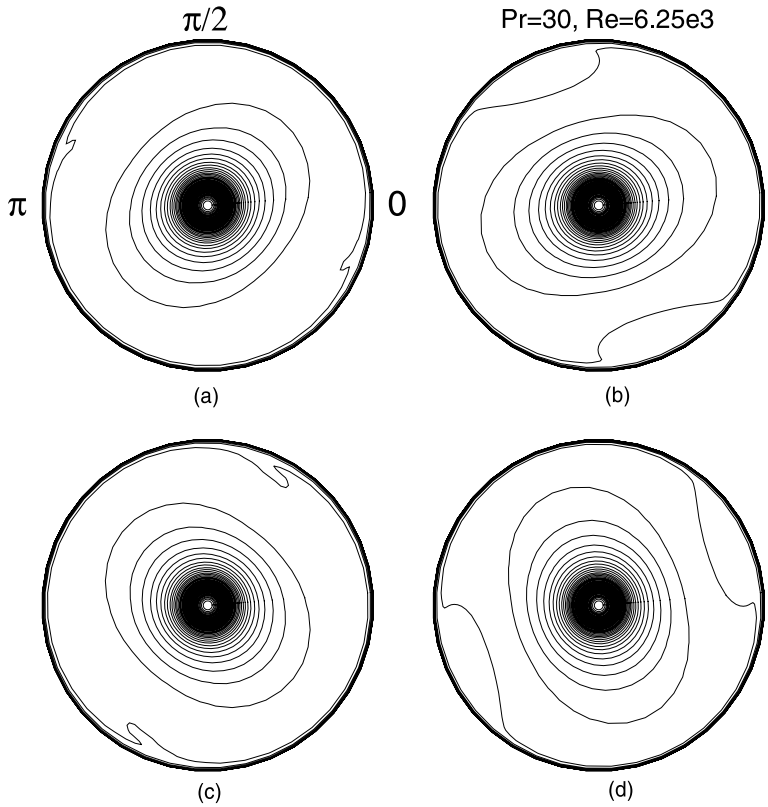


Fig. 8. One cycle of temperature oscillations at the free surface associated with Fig. 7(a). The frequency of the pulsating pattern is twice that of the temperature oscillations.

consist of two pairs of hot and cold spots, i.e. two azimuthal waves, and the spots are pulsating at the azimuthal positions ($\theta = \pi/6$ and $2\pi/3$). It is shown from Figs. 8 and 9 that the temperature at the free surface is invariant to a $\theta$ rotation of $\pi$, indicative of a wavenumber of two.

Supercritical temperature distributions at the free surface and the meridional plane ($\theta = 0$) with various $Re$ are shown in Fig. 10. The pulsating pattern remains unchanged with increasing $Re$ beyond the critical value. This pattern on the free surface is very different from those of open annuli heated from the inside wall [6,8], where a two-lobed rotating wave near the critical region is replaced by a two-lobed pulsating or a three-lobed rotating wave as $Re$ increases.

While experimental studies of oscillatory thermocapillary convection with $Pr = 30$ (2 cSt silicone oil) were reported, oscillatory convection with $Pr = 97$ (10 cSt silicone oil) was not. Experiments [3] with $Pr = 97$ were performed up to $Re = 5200$, and only steady thermocapillary convection was observed. We compute $Re_c$ of about $8.5 \times 10^3$ which is consistent with the experiment. When compared with $Pr = 30$, $Ma_c$ is about five times higher. This is probably due to increased viscous effects at higher $Pr$. Because the flow pattern is similar to the case of $Pr = 30$, the plots with $Pr = 97$ are omitted here. Fig. 11 shows the variation of critical $Re$ and $F$ with $Pr$. While $Re_c$ increases with increasing $Pr$, the critical frequency, $F_c$, decreases with increasing $Pr$. Agreement with available results from experiment [5] is indicated.

### 4.3. Three-dimensional thermocapillary convection with a concave surface

$Re_c$ with $V = 0.81$ and $Pr = 30$ is computed at about $2.3 \times 10^4$, which is well within the experimentally determined range ($1.67 \times 10^4$–$2.86 \times 10^4$) [17]. Fig. 12 gives temperature distributions for one cycle of oscillations at the free surface when $Re = 2.5 \times 10^4$. It can be seen that three azimuthal waves are rotating clockwise. The isotherms have the same shape when rotated by $2\pi/3$. Thus the oscillation frequency is three times the isotherm rotation frequency. The temperature fluctuations in one cycle are shown in Fig. 13. Three pairs of hot and cold spots, i.e. three azimuthal waves, are observed on the free surface, and the spots are rotating clockwise as shown in Fig. 13. With increasing $Re$

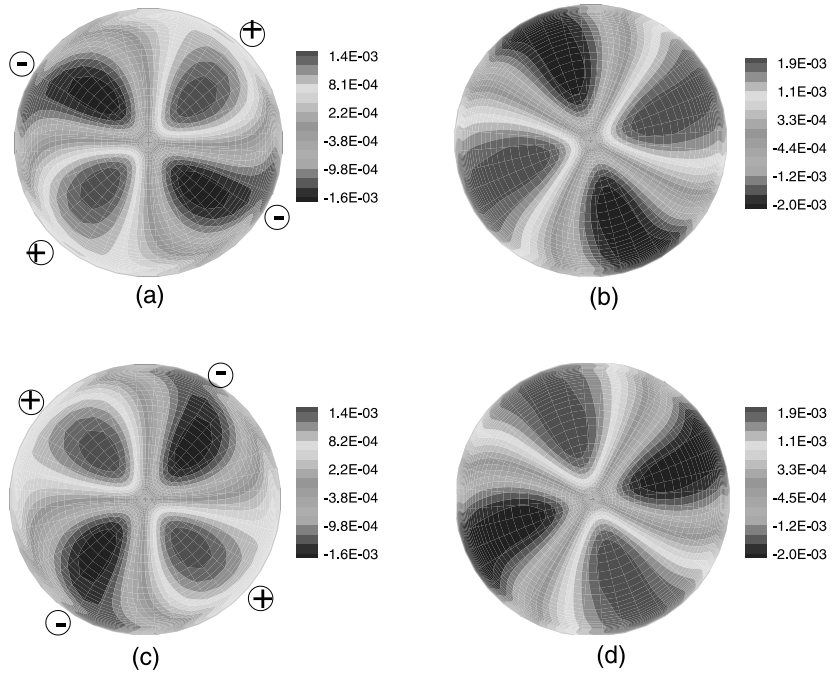


Fig. 9. Snapshots of free surface temperature fluctuations (deviation from the time-average at each position) at four instances within one cycle corresponding to Fig. 8. Two pairs of hot and cold spots are pulsating at the azimuthal positions ($\theta = \pi/6$ and $2\pi/3$) in (b) and (d).

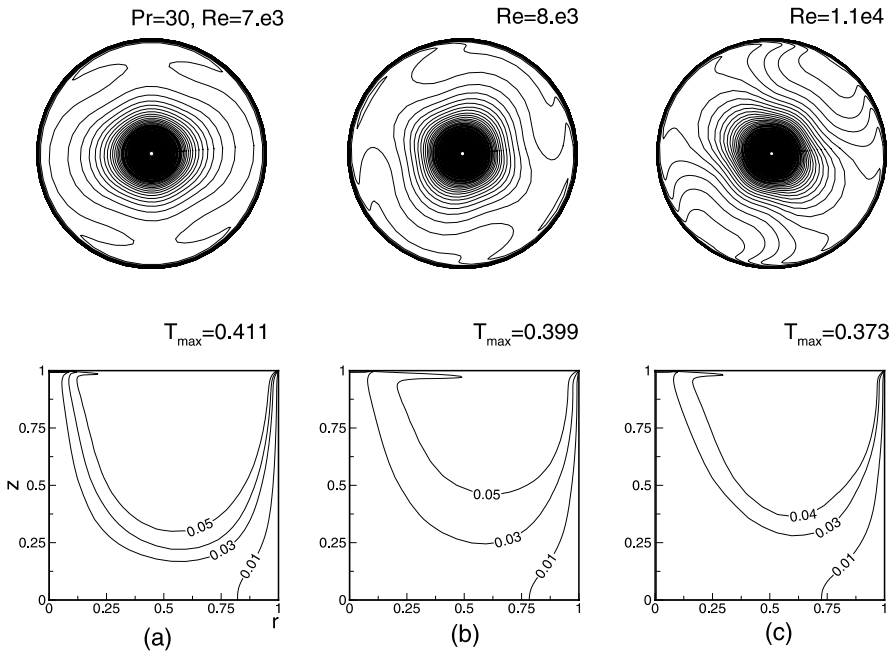


Fig. 10. Temperature distributions on the free surface and the meridional plane ($\theta = 0$) with $Pr = 30$, $V = 1$ and increasing $Re$. The pulsating pattern prevails.

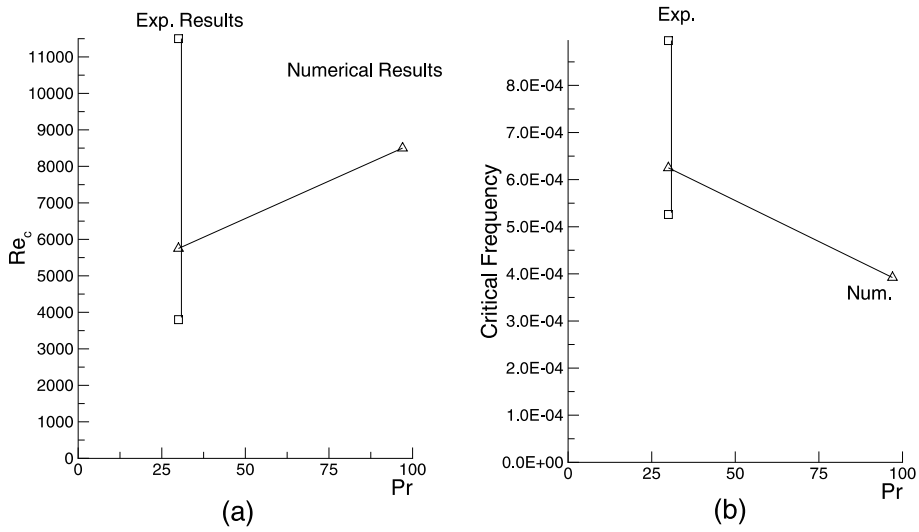


Fig. 11. Critical (a) Reynolds numbers and (b) frequencies of temperature oscillations corresponding to $V = 1$ and various $Pr$. While $Re_c$ increases with increasing $Pr$, $F_c$ decreases.

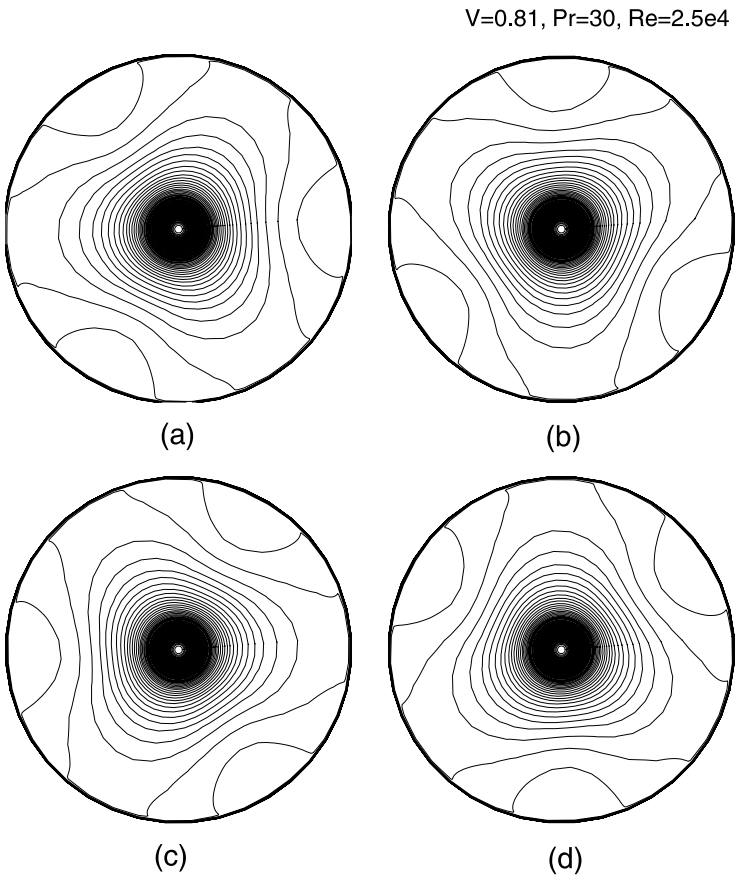


Fig. 12. One cycle of temperature oscillations at the free surface with $Pr = 30$, $V = 0.81$ and $Re = 2.5 \times 10^4$. Three azimuthal waves are rotating clockwise on the free surface (two-dimensional plot).

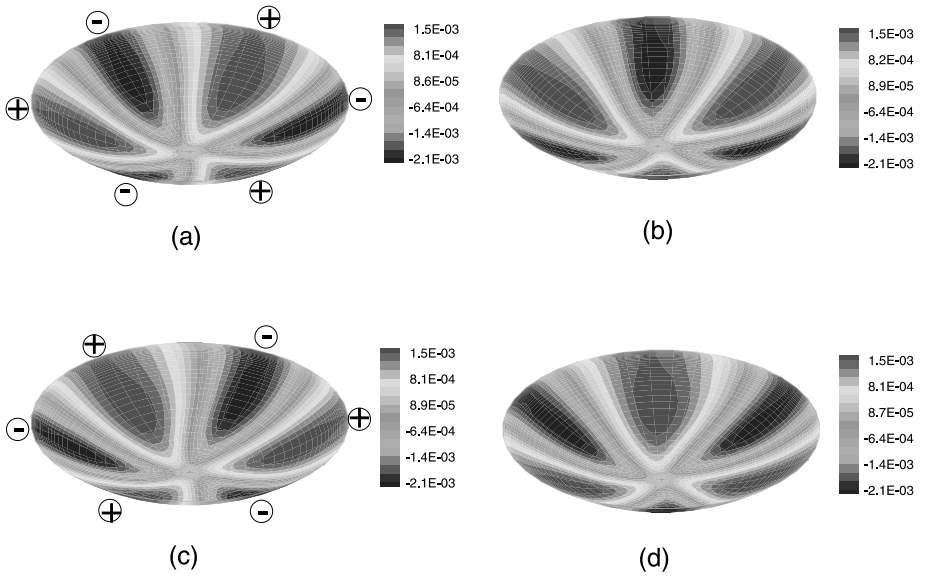


Fig. 13. Three-dimensional snapshots of free surface temperature fluctuations (deviation from the time-average at each position) at four instances within one cycle corresponding to Fig. 12. Three pairs of hot and cold spots are rotating clockwise.

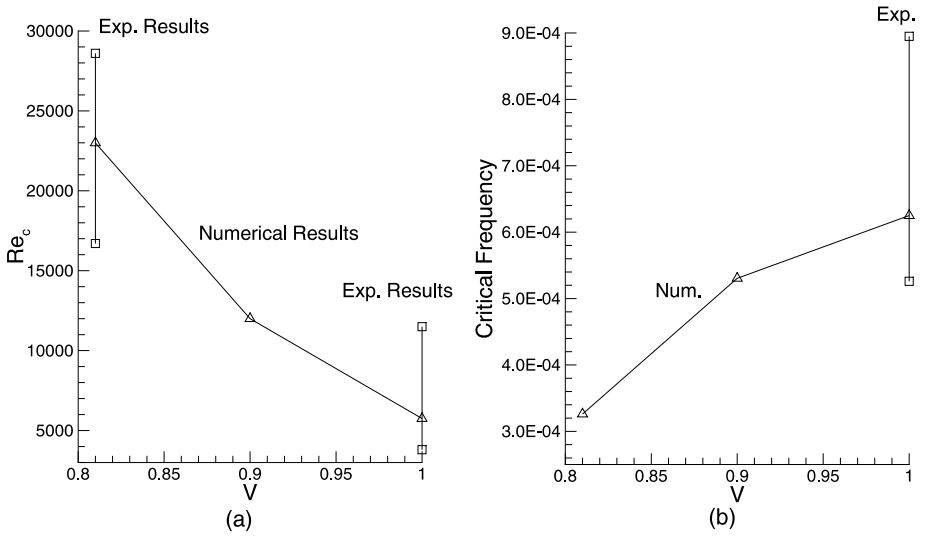


Fig. 14. Critical (a) Reynolds numbers and (b) frequencies of temperature oscillations corresponding to $Pr = 30$ and various $V$. While $Re_c$ decreases with increasing $V \leqslant 1$, $F_c$ increases.

beyond $Re_c$, the three rotating waves remain unchanged up to $Re = 4.3 \times 10^4$.

$Re_c$ with $V = 0.9$ and $Pr = 30$ is about $1.2 \times 10^4$, and the wave pattern on the free surface is also rotating clockwise with three azimuthal waves. Fig. 14 shows the variation of $Re_c$ and $F_c$ with $V$. The numerical $Re_c$ with $V = 0.81$ is in agreement with the experimental results [17], however $F_c$ from the experiment was not reported. While $Re_c$ decreases with increasing $V$, $F_c$ increases with increasing $V$.

## 5. Conclusions

Two- and three-dimensional thermocapillary convection driven by a uniform heat flux in an open cylinder of unit aspect ratio is investigated numerically to document its stability characteristics. Two-dimensional simulations with flat or curved free surfaces predict steady convection even at very high $Re$. It is found that only azimuthal waves can generate oscillations in thermocapillary convection. While the maximum nondimensional

surface velocity and temperature decrease with increasing $Re$ or $Pr$, they are independent of the liquid volumes for the parameter values we considered.

Oscillatory thermocapillary convection is possible only in three-dimensional calculations. This is consistent with experiments. As expected, starting from the same steady state initial conditions, oscillations begin earlier in time at higher $Re$. While the amplitudes of temperature oscillations are larger at higher $Re$, the mean temperature is found to decrease with increasing $Re$. With a flat free surface, two-lobed pulsating waves are found on the surface with $Pr = 30$ and 97. The wave is pulsating twice for one cycle of temperature oscillation. The pulsating pattern remains unchanged with increasing $Re$ beyond the critical value. While $Re_c$ increases with increasing $Pr$, $F_c$ decreases. In the case of a concave free surface with $V = 0.81$, three azimuthal waves are found rotating clockwise on the surface. While $Re_c$ decreases with increasing $V$, $F_c$ increases. The results are in reasonable agreement with available experiments.

## Acknowledgements

We gratefully acknowledge computer resources from the Rutgers Computational Grid composed of a Distributed Linux PC Cluster on which all computations were performed.

## References

[1] D. Schwabe, U. Moller, J. Schneider, A. Scharmann, Instabilities of shallow dynamic thermocapillary liquid layers, Phys. Fluids 4 (1992) 2368–2381.
[2] D. Schwabe, Microgravity experiments on thermocapillary flow phenomena: examples and perspectives, J. Jpn. Soc. Microgravity Appl. 16 (1999) 1–6.
[3] Y. Kamotani, S. Ostrach, A. Pline, A thermocapillary convection experiment in microgravity, J. Heat Transfer 117 (1995) 611–618.
[4] Y. Kamotani, S. Ostrach, A. Pline, Analysis of velocity data taken in surface tension driven convection experiment in microgravity, Phys. Fluids 6 (1994) 3601–3609.
[5] Y. Kamotani, S. Ostrach, J. Masud, Oscillatory thermocapillary flows in open cylindrical containers induced by $CO_2$ laser heating, Int. J. Heat Mass Transfer 42 (1998) 555–564.
[6] Y. Kamotani, S. Ostrach, J. Masud, Microgravity experiments and analysis of oscillatory thermocapillary flows in cylindrical containers, J. Fluid Mech. 410 (2000) 211–233.
[7] M. Mundrane, A. Zebib, Low Prandtl number Marangoni convection with a deformable interface, AIAA J. Thermophys. Heat Transfer 9 (1995) 795–797.
[8] B.-C. Sim, A. Zebib, Effect of surface heat loss and rotation on transition to oscillatory thermocapillary convection, Phys. Fluids 14 (2002) 225–231.
[9] D. Schwabe, A. Zebib, B.-C. Sim, Oscillatory thermocapillary convection in open cylindrical annuli. Part 1. Experiments under microgravity, J. Fluid Mech., submitted for publication.
[10] B.-C. Sim, A. Zebib, D. Schwabe, Oscillatory thermocapillary convection in open cylindrical annuli. Part 2. Simulations, J. Fluid Mech., submitted for publication.
[11] J. Keller, T. Bergman, Thermocapillary cavity convection in wetting and nonwetting liquids, Numer. Heat Transfer A 18 (1990) 33–49.
[12] Y. Kamotani, J. Platt, Effect of free surface shape on combined thermocapillary and natural convection, AIAA J. Thermophys. Heat Transfer 6 (1992) 721–726.
[13] A. Liakopoulos, G. Brown, Thermocapillary and natural convection in a square cavity, in: Proceedings of ASME Winter Annual Meeting, New Orleans, LA, ASME-AMD, 170, 1993, pp. 57–73.
[14] M. Mundrane, J. Xu, A. Zebib, Thermocapillary convection in a rectangular cavity with a deformable interface, Adv. Space Res. 16 (7) (1995) 41–53.
[15] J. Chen, J. Sheu, S. Jwu, Numerical computation of thermocapillary convection in a rectangular cavity, Numer. Heat Transfer A 17 (1990) 287–308.
[16] J. Chen, F. Hwu, Oscillatory thermocapillary flow in a rectangular cavity, Int. J. Heat Mass Transfer 36 (1993) 3743–3749.
[17] Y. Kamotani, S. Ostrach, J. Masud, Conditions for the onset of oscillatory thermocapillary flows in cylindrical containers with $CO_2$ laser heating, 35th Aerospace Sciences Meeting and Exhibit, Reno, NV, 1997, AIAA 97-0889.
[18] M. Lappa, R. Savino, R. Monti, Three-dimensional numerical simulation of Marangoni instabilities in non-cylindrical liquid bridges in microgravity, Int. J. Heat Mass Transfer 44 (2001) 1983–2003.
[19] B.-C. Sim, Thermocapillary convection in cylindrical geometries, Ph.D. Thesis, Rutgers University, New Brunswick, NJ, 2002.
[20] V. Shevtsova, J. Legros, Oscillatory convective motion in deformed liquid bridges, Phys. Fluids 10 (1998) 1621–1634.
[21] J. Xu, A. Zebib, Oscillatory two- and three-dimensional thermocapillary convection, J. Fluid Mech. 364 (1998) 187–209.